

ORIGINAL ARTICLE

Open Access



Surface deformation of northeastern Taiwan revealed by geomorphic indices

Chin-Yi Yang^{1*} , Ting-Wei Huang¹, Chung-Pai Chang² and Pei-Shan Hsieh¹

Abstract

In northeast Taiwan, many areas are affected by various tectonic forcings. Some areas appear to have a subsidence tendency, whereas others reflect uplift activities on the surface, due to tectonic northward compressive forcing growth and decline. Owing to the presence of widespread mountain areas, limited geodetic surveys in the field have made data scarce in the study area in the past decades. The distribution of the geomorphic indices, which were calculated along the river channels, were used to analyze the activities on a regional scale in this study. The long-term landscape evolution of drainage basins can record topographic changes through the river channels. By calculating the location and drop height of knickpoint in the river longitudinal profile, as well as the spatial distribution of the normalized steepness index (K_{sn}) value, it is possible to comprehensively discuss the perturbations that were caused by possible factors in river channels. Our results from the geomorphic indices synthetically suggest that the river channel of drainage basins is mainly influenced by the perturbations such as geological structures, tectonic activity, various lithologies, potential ruptures. In the study area, tectonic forcing act on a large area from north to south, which is reflected in the long-term incision of the river into the bedrock. Moreover, the potential ruptures on the surface may also induce displacement in the local area.

Key points

- The geomorphic indices reveal surface deformation on a regional scale.
- The long-term perturbations caused by endogenetic process on river channels.
- The landscape evolution model was generalized based on the result of the geomorphic indices.

Keywords Geomorphic indices, Landscape evolution model, Northeastern Taiwan

1 Introduction

Taiwan is situated at the convergent boundaries between the Philippine Sea Plate (PSP) and the Eurasian Plate (EUP), where the northwestward convergence rate is approximately 80 mm/yr (Yu et al. 1997) resulting in southward subduction and collisional processing on the island. The western edge of the PSP (WEP) boundary is beneath northern and northeastern Taiwan (Wu et al. 2009; Su et al. 2019). The oblique projected WEP boundary across these areas might reflect different tectonic activities on the surface. The Nanao, Heping, Heren and Liwu drainage basins were chosen as the study areas,

*Correspondence:

Chin-Yi Yang
chinyiyang@itri.org.tw

¹ Material and Chemical Research Laboratories, Industrial Technology Research Institute, No. 195, Sec. 4, Zhongxing Rd., Zhudong, Hsinchu 310401, Taiwan

² Center for Space and Remote Sensing Research, National Central University, Jhongli, Taoyuan, Taiwan



all of which are located in northeastern Taiwan (Fig. 1a). From north to south, these drainage basins experience post-collision to the collision initial stage of the neotectonic domain (Chen et al. 2015). The WEP boundary projects oblique to the ground surface through the Heping and Liwu drainage basins (Fig. 1b). In particular, most of the Liwu drainage basin is on the left side of the WEP-projected boundary, which might represent this area experiencing the tendency of uplift.

In northeast Taiwan, the precipitous topography makes it difficult to measure the land surface vertical movements from recent geodetic surveys (GNSS and levelling measurements), and these surveys of previous results almost continue along the coastline at present (Ching et al. 2011). Furthermore, the mountainous topography and dense vegetation in this area have restricted effectiveness of using InSAR technology in the laboratory for analyzing surface deformation. In the drainage basins of study area, most upstream streams originate from the Backbone Range (Fig. 1a) and immediately flow into the ocean. Because of the steep topography, field investigations on land have been restricted, and *in-situ* surveys

are usually limited. This might lead to the possibility that active structures have not been recorded in this area in the published geological maps. Due to the presence of widespread mountain areas that limit geodetic surveys in the field, data from the past decades are scarce in some areas of northeast Taiwan. Recently, the Industrial Technology Research Institute (ITRI) established continuous GNSS stations and carried out regular levelling measurements in this area. These data are restricted to the confidential protocol and remain unpublished. Instead, this study uses the topographic data to conduct a series of quantitative analysis to obtain the surface deformation information in the study area.

The longitudinal profiles of bedrock rivers may yield valuable information regarding the distribution of recent deformation within the underlying region (Duvall et al. 2004). Because the river network can extend over the entire drainage basin, long-term river incision into bedrock can record topographic changes through river channels (Duvall et al. 2004; Gallen et al. 2013; Jaiswara et al. 2020; Kirby and Whipple 2012; Perron and Royden 2013; Wang et al 2019). In this study, we attempted to analyze

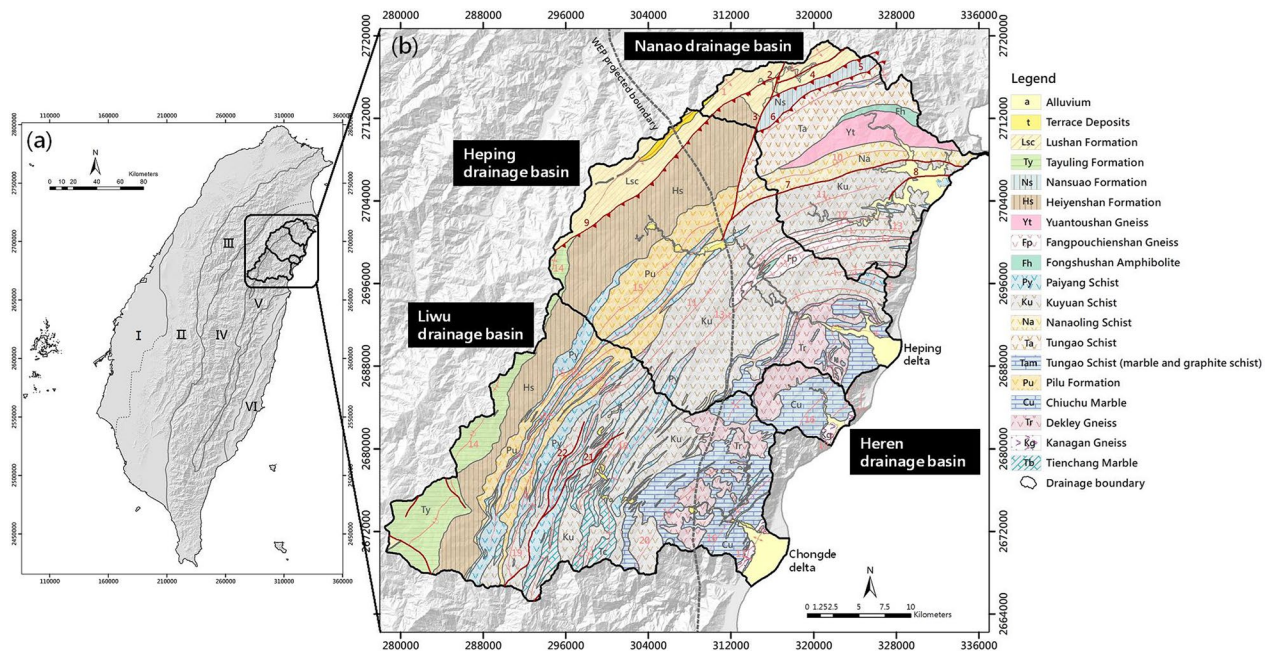


Fig. 1 **a** The location of the Nanao, Heping, Heren and Liwu drainage basins in Taiwan. The roman numbers on the map (modified from Chen et al. (2016)) represent different geological zones. I: Coastal Plain; II: Western Foothills; III: Hsuehsan Range; IV: Lushan Slate Belt of the Backbone Range; V: Tananao Schist Belt of the Backbone Range; VI: Coastal Range. **b** The base map is modified referring to the geological map from “Geological Investigation & Database Construction for Upstream of Flood-Prone Area” (Fei and Chen 2013). The boundary of faults, anticlinoria, synclinoria, and lithology units also refer to the geological map. The abbreviations indicate the individual lithology units. Numbers next to the lineament structure on the map indicate the following: 1. Sanxingshan Anticlinorium; 2. Tsueyfenghu Fault; 3. Kulu Fault; 4. Umaoshan Fault; 5. Houishan Fault; 6. Wansueyshan Fault; 7. Lupihsi Fault; 8. Nanao Fault; 9. Meichi Fault; 10. Lupihsi Synclinorium; 11. Loshao Synclinorium; 12. Fangpouchienshan Anticlinorium; 13. Tienhsiang anticlinorium; 14. Dayuling Synclinorium; 15. FunPeishan Synclinorium; 16. Qingshui Synclinorium; 17. Heren Anticlinorium; 18. Kuyuan Anticlinorium; 19. Paiyan Anticlinorium; 20. Sanzhui Anticlinorium; 21. Dishan Fault; 22. Loshao Fault. The grey dashed line represents the WEP boundary projected to the map (Wu et al. 2009; Su et al. 2019)

geomorphic indices that can provide observations on a regional scale to discuss the long-term tendency of landscape evolution in drainage basins. The characteristics of topography changes can be reflected by the geomorphic indices, and the perturbations in the river channels can be generated from several factors. The various factors that acted on river channel may be related to tectonic activity, various lithologies, possible structures, or potential surface ruptures in the Nanao, Heping, Heren and Liwu drainage basins.

2 Geological and geomorphologic background

Our study area includes the Nanao, Heping, Heren and Liwu drainage basins from north to south (Fig. 1a, b). The terrain is composed of alluvial fans, steep cliff coast, and mountains, and the topographic elevation increases gradually from northeast to southwest. Many short and steep streams flow along the east coast of the study area. The east side of these drainage basins has steep coastal cliffs, and most of the streams that originate from the eastern flank of the Central Range flow roughly from west to east into the Pacific Ocean. The estuaries of the Nanao, Heping and Liwu Rivers have the alluvial fans consisting of gravel, mud, and sand, and the Heping and Chongde delta fans are larger in the study area.

In accordance with the geological map (Fig. 1a), these drainage basins are located in the Backbone Range, which consists of the Tananao Schist Belt and Lushan Slate Belt. Several lithology types are distributed in the studied drainage basins according to the geological map published by the Central Geological Survey (Fei and Chen 2013) (Fig. 1b). The ages of the lithologic units range from the Late Paleozoic to the Holocene. The lithology in the study area comprises mainly metamorphic rocks such as slate, gneiss, schist, marble, and amphibolite, and the lithology units expose complicated configurations on the surface among the studied drainage basins.

The Nanao drainage basin is located in Ilan County, north of the Heping drainage basin, and originates from the Sansing Mountain, accompanied by the Nanao North and South Stream convergence (Fig. 2). The convergence of the two streams gradually forms an alluvial plain towards the estuary with a lower elevation (<50 m) southeast of the Nanao drainage basin. The area of the Nanao drainage basin is 311.73 km², and the main channel is 48.40 km long. Most of the Nanao drainage basin is composed of schist, and the northern side is dominated by Lushan (Lsc) Formation and Nansuao (Ns) Formation. Other lithologies include alluvium, gneiss, and amphibolite; in particular, Yuantoushan (Yt) Gneiss and Fongshushan (Fh) Gneiss emerged only in this drainage basin (Fig. 1b).

The Heping drainage basin is composed of the Heping North and South Stream, and originates from the Nanhu Mountain across Ilan and Hualien County, south of the Nanao drainage basin (Fig. 2). The Heping drainage basin area is 561.06 km², and the main channel is 48.20 km long. The Heping North Stream, also known as the Dazhuoshui Stream, has experienced many landslides along the channel, leading to large sediment discharge and turbidity in the streams. As for the valley of Heping South Stream, it is mostly characterized by deep and narrow topography, good forest growth, infrequent landslides, and relatively clear and abundant water. It also appears as a large alluvial fan at the river mouth of the Heping drainage basin due to the elevation dropping within a short distance along the river, which causes erosion and landslides upstream. The lithological units of the Heping drainage include Lsc Formation, Heiyenshan (Hs) Formation, Tungao (Ta) Schist, Nanaoling (Na) Schist, Fangpouchienshan (Fp) Gneiss and Kuyuan (Ku) Schist and are extensions from the Nanao drainage. Others, such as the Tayuling (Ty) Formation, Pilu (Pu) Formation, Dekley (Tr) Gneiss and Chiuchu (Cu) Marble, begin to stretch southward from this drainage basin (Fig. 1b).

The Heren drainage basin adjacent to the southeastern side of the Heping drainage basin has the smallest area (51.70 km²) compared to the other drainage basins in this study (Fig. 2). The main channel from the estuary of the Heren River is approximately 16 km long with a steeper gradient, and the river network is short and uncomplicated. The Google Earth image exhibits large debris slumps and slides, and debris flows surrounding the fringes of the Heren drainage basin. The lithologic units in this drainage basin are made up of Tr Gneiss, Cu Marble, Kanagan (Kg) Gneiss (Fig. 1b).

The Liwu drainage basin is located south of the Heping drainage basin and is a well-known drainage basin site in Hualien County. The Liwu River originates between the Central Mountain Range and the Hehuan Mountain. The Liwu drainage basin area is 630.38 km², and the main channel is approximately 55 km long. The incision topography of the Taroko Gorge, with a drop elevation of more than 1000 m was shaped by the Liwu River. The four tributaries spread in the upper-middle reaches of the Liwu drainage basin are the Tausai, Saowaheru, Waheru and Liwu Streams (Fig. 2). The lithological units expose the most complicated configuration in this drainage basin. Except for the Tr Gneiss and Cu Marble lithologies, which expose large blocks to the east of this drainage basin, other lithology units are inlaid in each other and distributed in a northeast-southwest direction stripe shape (Fig. 1b).

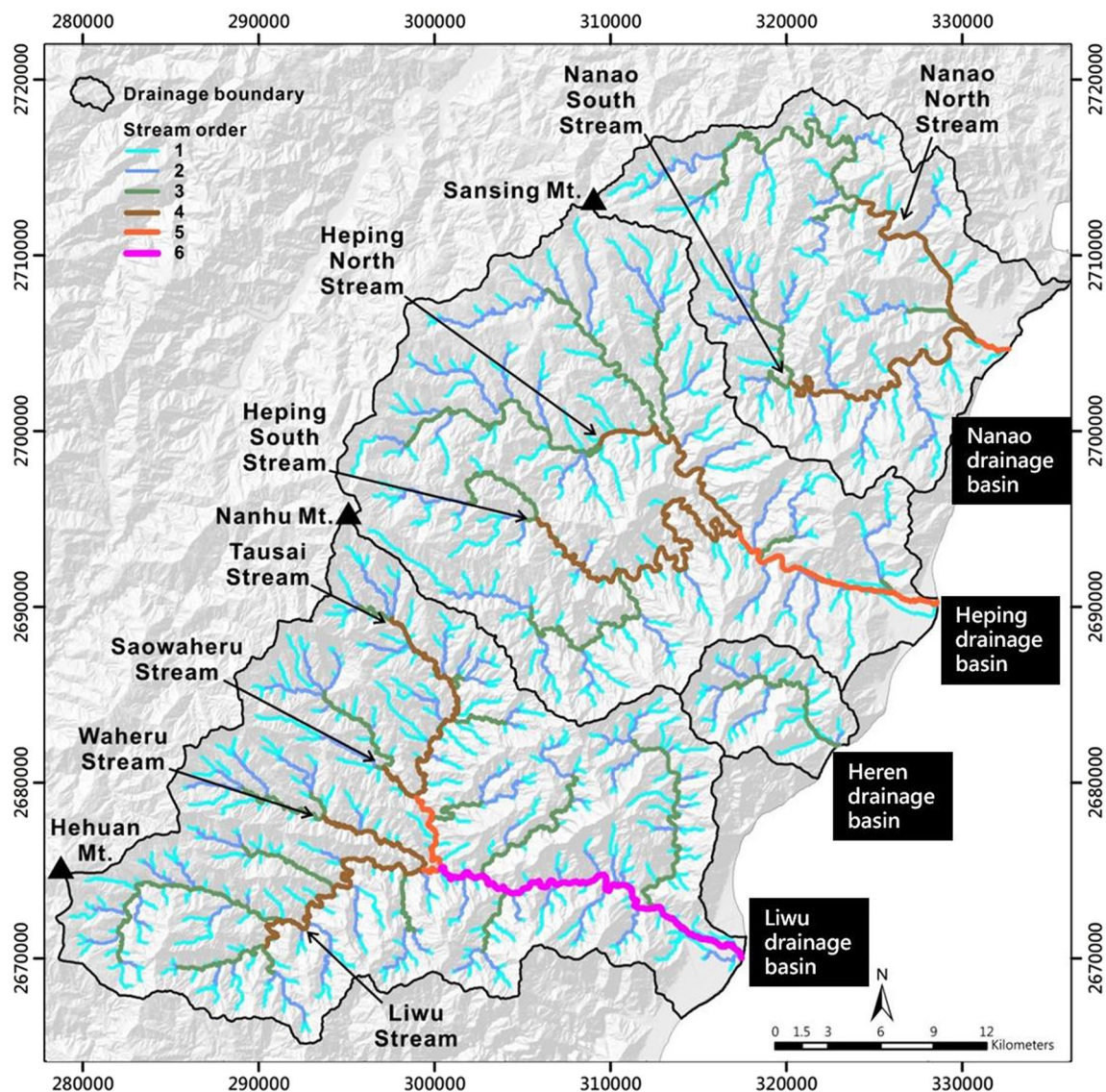


Fig. 2 The expansion river channels including the stream order (1 to 6) of the river network. The stream order follows the method of Strahler (1952)

As previously mentioned, the WEP boundary projects oblique to the ground surface through the Heping and Liwu drainage basins. The Nanao drainage basin is on the north side of the projected WEP boundary, which means that it has already passed the collision stage and might experience ongoing subsidence. The Heping and Liwu drainage basins were affected by tectonic implications, which might present complicated topographic relief. Because the east side of the WEP projected boundary could still be under the influence of tectonic uplift activity, we conducted this study to find relevant evidence.

3 Data and methodology

3.1 Drainage network extraction and digital elevation model (DEM) processing

In this study, we used the DEMs with a spatial resolution 20 m georeferenced TWD97 published by the Ministry of the Interior (MOI) in 2018 to extract the river drainage network. The individual drainage basin boundary depended on open information from the public platform of the Water Resources Agency (WRA) (<https://gic.wra.gov.tw/gis/>). The function library TopoToolBox2 was used to calculate the flow direction, river network, location of knickpoints, and steepness index of the drainage

basin. TopoToolBox2 (Schwanghart and Scherler 2014, 2017) provides essential tools for large scale geomorphological approaches, and the algorithm performed to derive drainage network extraction from DEM is the single flow direction (SFD) algorithm. The accumulation map is computed by the SFD algorithm, which provides the drainage basin area upstream of each pixel of the DEM and allows the selection of the network extension by defining a threshold source area (Simoes et al. 2021). The extension of the drainage network configuration was adopted for comparison with the river configuration on a geological map (Fei and Chen 2013) during the extraction process. The more streams on the geological map, the fewer the threshold contributing pixels (which can also be converted to the threshold source area) in the algorithm. However, the extracted configuration of the drainage network did not exactly match the geological map, and the extraction process needed to execute several tests to obtain the appropriate threshold contributing pixels. After comparison with the geological map, the threshold contributing pixels of the Nanao and Heping drainage networks were both determined to be 2000, and the Heren and Liwu drainage networks were determined to be 1000 pixels.

3.2 River knickpoints extraction

The knickpoint of the channel longitudinal profile is the location where sharp convexities exist in a concave-up longitudinal profile. The form and behavior of knickpoints that discreet changes in the steepness of the river longitudinal profile depend on both the nature of the perturbation and mechanics of the river incision (Kirby and Whipple 2012). The function of TopoToolBox2 selects knickpoints by creating reference channel longitudinal profiles that are concave up and then selecting knickpoints for which the actual channels are the most different from the reference channels. This method is well adapted for identifying specific types of knickpoints and does not allow for the separate identification and quantification of positive slope-break, negative slope-break and vertical-step knickpoints (Gailleton et al. 2019). A sensitivity parameter defines the number of iterations, and indirectly, the number of knickpoints detected (Gailleton et al. 2019). Identification tolerance refers to the final vertical offset between the true and idealized longitudinal profiles at the location of the knickpoint (Palézieux et al. 2020). Reducing the tolerance parameter increases the number of detected knickpoints (Gailleton et al. 2019). Each drainage basin has various tolerances, owing to the range of the DEM data spikes inherent along the channel longitudinal profile. To estimate the tolerance appropriate for the longitudinal profiles of the entire drainage basin, the range between the downstream minimum and

upstream maximum spikes was calculated. This approach was adapted to the maximum difference between elevations, which is the maximum relative error estimated from the profile. Based on the topography and quality of the DEM, we suggest that the tolerance parameter be estimated individually for each drainage basin.

3.3 River longitudinal profile smoothing

The quantile carving and constrained regularized smoothing (CRS) algorithms of TopoToolBox2 were applied in the DEM smoothing process before analysis. These quantile regression techniques enable the hydrological correction and uncertainty quantification of river longitudinal profiles (Schwanghart and Scherler 2017). Small-scale topographic noise associated with DEM artifacts along river paths can be eliminated using the CRS algorithm (Simoes et al. 2021). The smoothing parameter (k) and quantile (τ) are the primary parameters used to reconstruct the denoising profile along the river longitudinal profile. The τ parameter is derived by sorting the data and determining the values that separate the data into the desired proportions. Another parameter, k , influences the longitudinal profile smoothing. The smoother longitudinal profile results from the larger value of k . A higher k value more effectively filters the longitudinal profile but strongly influences the range between the 10th and 90th percentiles at some locations. Adjusting k to increase its value can excessively smooth the longitudinal profile and thus impair the agreement between the elevations and gradients of the longitudinal profile. Very low and high values of τ can also lead to grave mismatches of the smoothed longitudinal profile (Schwanghart and Scherler 2017). Previous research has also pointed out that the agreement between elevations or slopes is not necessarily derived from the same set of parameter values. Agreement of elevations is largely obtained by varying τ in a rather broad range of k between 0.1 and 3, agreement of gradients is largely within a narrow range of k and a broad range of τ between 0.3 and 0.8 (Schwanghart and Scherler 2017). Fitting longitudinal profiles may significantly depend on minimizing the differences between river elevations or gradients. The CRS algorithm can be implemented in the entire river network (Zhou et al. 2021). In this study, the large-scale drainage basin was taken into consideration, and the main channels and tributaries of the entire drainage basin were both synchronously included in the calculation. The entire river longitudinal profile of the main channel and its tributaries exhibit significant varies in elevation and gradient. Additionally, each drainage basin is composed of different small watersheds, and the river longitudinal profile in these watersheds also varies in elevation and gradient. Therefore, from the large-scale drainage basin to the small-scale watersheds, not only the elevation and gradient differ in each river longitudinal profile but

also exists many spikes noises on DEM. The river longitudinal profiles of the main channel and its tributaries exhibit an undulated elevation and irregular shape. Regarding the library TopoToolBox2 suggested default value, we used the set of median τ value ($\tau=0.5$) and $k=2$ for the calculation process of the CRS algorithm in these drainage basins.

3.4 Normalized steepness index calculation

In a bedrock river profile, the profiles following the stream power river incision model tend to reach a graded shape by adjusting the upstream discharge and transport load (Whipple 2004). The evolution of bedrock river profiles is usually formed by competition between uplift and erosion (Howard et al. 1994; Whipple and Tucker 1999):

$$\frac{dz}{dt} = U - E = U - KA^m S^n \tag{1}$$

where dz/dt is the change in elevation of the river channel with time, U is the uplift rate relative to the reference elevation, E is the bedrock erosion, K is the erosion coefficient, A is the upstream drainage area, S is the channel gradient, and m and n exponents are positive constants that reflect basin hydrology, hydraulic geometry, and erosion process (Howard et al. 1994; Whipple and Tucker 1999).

The river topography appears as an equilibrium profile when it reaches a steady state and the term dz/dt change is zero:

$$\frac{dz}{dt} = U - E = U - KA^m S^n = 0 \tag{2}$$

The graded river profiles can be defined by a power-law relationship between the channel gradient (S) and upstream drainage area (A) (Jaiswara et al. 2020).

$$S = \left(\frac{U}{K}\right)^{1/n} A^{-m/n} = k_s A^{-\theta} \tag{3}$$

where the coefficient of the power law includes the ratio $\left(\frac{U}{K}\right)^{1/n}$ of these two parameters, referred to as the steepness index (k_s), which controls the overall gradient of the channel and changes with the elevation gap. The k_s index increases when the gap is larger for the equivalent river length. Because k_s is simplified from U and K , it is considered to reflect relative regional uplift (Marliyani et al 2016). A denotes the upstream drainage area, and θ (m/n) represents the intrinsic concavity of the channel profiles because a higher value leads to a more rapid channel gradient decrease downstream (Duvall et al. 2004; Gailleton et al. 2019).

Because of the high correlation between k_s and θ , the variation in θ is likely to affect the result of k_s .

Hence, the normalized steepness index (K_{sn}) must be used to describe this autocorrelation. Most previous studies have generally cited θ_{ref} as 0.45 (Wobus et al. 2006). The K_{sn} with a reference concavity to correlate catchments of various shapes and sizes is represented as follows:

$$K_{sn} = SA^{\theta_{ref}} \tag{4}$$

where θ_{ref} is the reference concavity averaged by the concavities of all channels in a drainage basin, and can be estimated by averaging the local θ value along the respective channels in the drainage basin. The reference concavity index typically falls into a relatively restricted range ($0.4 \leq \theta \leq 0.6$) in steady-state channels (Kirby and Whipple 2012). The K_{sn} value calculated from θ_{ref} can effectively compare the river profiles, which vary significantly in the drainage area between different drainage basins. The K_{sn} value, which can be a quantitative index of river topography and larger K_{sn} value reflects a greater change in the gradient of the river channel. In eastern Taiwan, the concavity index is also confirmed within the same range, and the reference concavity value ($\theta_{ref} = 0.45$) is calculated to obtain the K_{sn} along the river channels (Chen et al. 2015).

3.5 Identification of knickpoints from remote sensing image

The knickpoint with abrupt characteristics generated along the river longitudinal profile may be affected by numerous disturbance factors, and the locations of knickpoints need to be identified from remotely sensed data to recognize the possible factors effecting the surface. We utilized multitemporal Google Earth imagery to enhance the visual identification process. Through visual interpretation of remotely sensed images, many phenomena exhibited on the ground surface, such as landslide events (Ahmed et al. 2019), waterfalls, and artificial constructions that might form or influence knickpoint generation, can be checked simultaneously. In addition, landslide events prevailed, particularly in the Heping and Heren drainage basins observed from multitemporal Google Earth images. Moreover, the published landslide inventory (CGS 2016) also provides the historic landslide occurrences available for comparison. By comparing satellite images and landslide inventory, the locations of extracted knickpoints can be observed landslides have occurred along the river channel. Some landslides have occurred on one side of the river channel's slope, while others have occurred on surrounding river channel slopes, which can help us identify the occurrence of landslide events and the knickpoint generation might be influenced by the collapsed terrain in that location.

4 Results

4.1 Drainage network and knickpoint location

The Nanao drainage network is divided into two main separated tributaries, the Nanao North and South Stream. The Heping drainage network, also mainly separates into two tributaries, the Heping North and South Stream. The Heren drainage network reveals an apparently uncomplicated river system and a main channel flowing through almost the entire basin. The Liwu drainage network consists of many tributaries, including the Tausai, Saowaheru, Waheru and Liwu Streams (Fig. 2). The streams in a drainage network can be assigned orders. Higher stream order indicates more levels of branching in a river system. The Nanao and Heping drainage basins expand five grades of stream order; the Heren drainage basin only developed three grades of stream order; and the Liwu drainage basin with its complicated network grew up to six grades of stream order.

Compared with the Heping drainage basin, the distance of the main channel from the headwater to the estuary in the Nanao drainage basin is shorter, and the elevation is lower, almost below 2000 m. The extracted knickpoints of the Nanao drainage basin are mostly

located between elevations of 500 m and 1000 m (Figs. 3a, 4a and Table 1). The Heping drainage basin has the highest elevation (over 3200 m altitude) among four drainage basins (Figs. 3a and 4b). The extracted knickpoints of the Heping drainage basin have various drop height and they are almost distributed in throughout all elevation intervals. (Table 1 and Fig. 4b). Based on the longitudinal profile of the Heren drainage basin, it elevates rapidly at a short distance upstream, and the distribution of the extracted knickpoints of small to medium size lies in the lower elevation (< 800 m) (Figs. 3a and 4c). The spatial location of knickpoints with smaller magnitudes occurred in many tributaries of the Heren drainage basin (Fig. 3). The river longitudinal profile of the Liwu drainage basin displays that it has the most tributaries, and many tributaries have elevations above 2000 m. Most knickpoints with larger magnitudes are located at lower elevations (800–1500 m altitude) (Figs. 3a and 4d).

4.2 Magnitude of knickpoints distribution

The number of knickpoints extracted from the Nanao, Heping, Heren and Liwu drainage basins were 83, 130,

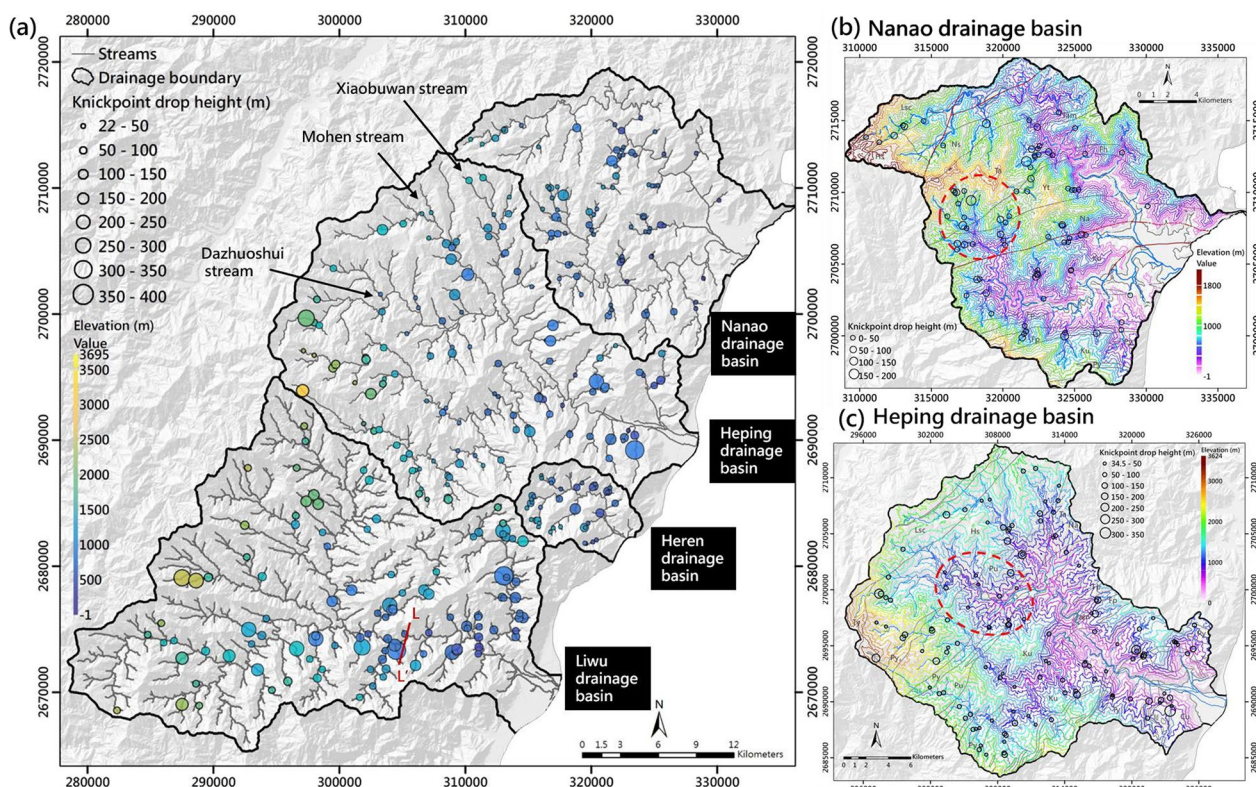


Fig. 3 a The extracted knickpoints with the magnitude of drop height and its elevation; The line L-L indicates the cross section of river channel topography; b knickpoints located at elevation contours in the Nanao drainage basin; c knickpoints located at elevation contours in the Heping drainage basin. The red dotted circle represents the cluster of knickpoints that may be induced by base-level lowering

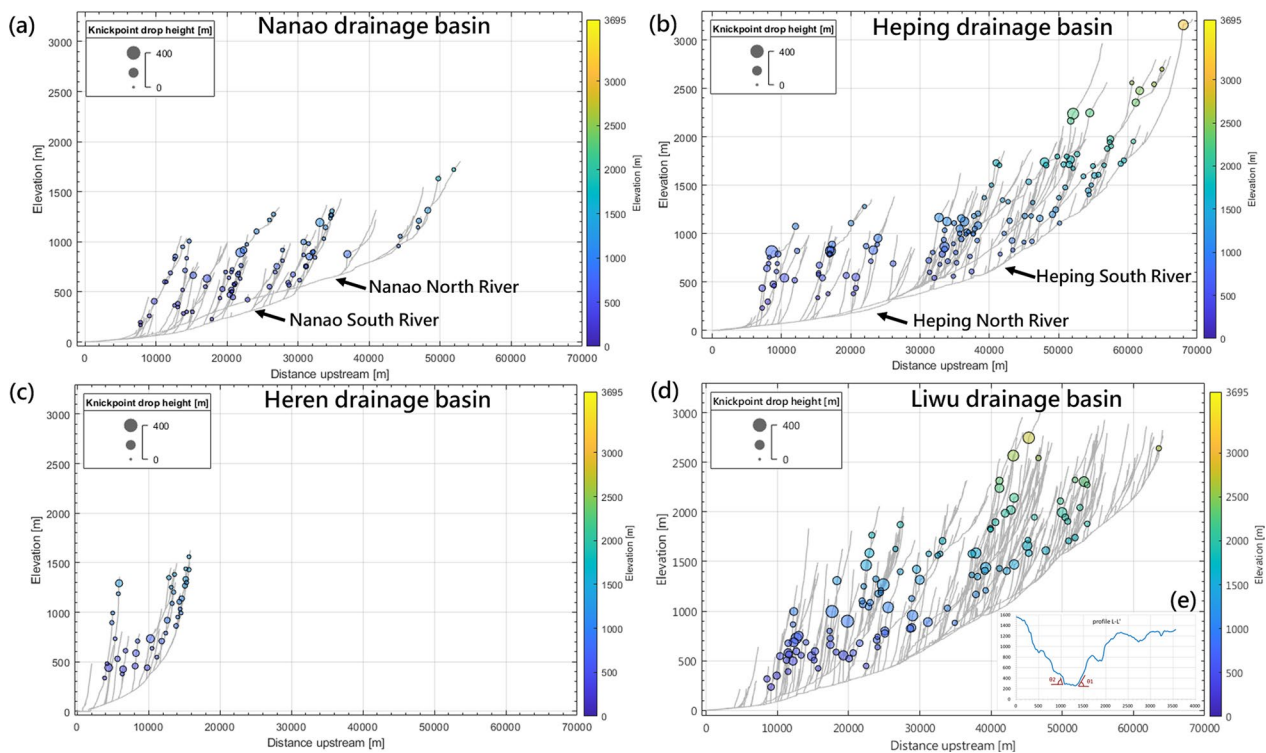


Fig. 4 The river longitudinal profile with the drop height of knickpoints on each drainage basin: **a** the Nanao drainage basin; **b** the Heping drainage basin; **c** the Heren drainage basin; **d** the Liwu drainage basin; **e** the river channel topography profile of line L-L' in Fig. 3a; the angle (θ_1) on the right side of the river channel is approximately 57° ; the angle (θ_2) on the left side of the river channel is approximately 61°

Table 1 The number of extracted knickpoints at elevation ranges in each studied drainage basin

Knickpoint elevation (m)	Nanao drainage basin	Heping drainage basin	Heren drainage basin	Liwu drainage basin
< 500	15	9	7	7
500–1000	49	54	16	36
1000–1500	16	32	15	27
1500–2000	2	26	1	25
2000–2500	–	5	–	9
2500–3000	–	3	–	4
Total number	83	130	39	108

39, and 108, respectively, and the tolerance parameters utilizing the extracted knickpoints were 22, 34, 28, and 64, respectively. The drop height (Δz) of the knickpoint was derived from a comparison with a reference longitudinal profile in the algorithm to quantify the magnitude of the offset between the reference and actual profiles. In the studied drainage basins, the magnitudes of most knickpoints manifested a small drop height (<100 m) (Table 2). The magnitude of the knickpoint indicates the degree of abrupt change in the river longitudinal profile,

and its possible causes provided the characterization of various geomorphic triggers on a regional scale. The smallest drop heights (<50 m) of knickpoints are generally distributed in the Nanao and Heren drainage basins, and there are also many knickpoints of this magnitude in the Heping drainage basin. The maximum number of knickpoints is in the range of 51–100 m drop height in the studied drainage basin. In the Heping and Liwu drainage basins with knickpoints of various magnitudes, particularly in the Liwu drainage basin, there are many knickpoints with larger drop heights. All knickpoint drop heights in the Nanao drainage are smaller than 200 m, whereas many knickpoints in the Liwu drainage basin have drop heights larger than 200 m. The distribution of the knickpoint drop height increases gradually from the Nanao drainage basin to the Liwu drainage basin (Figs. 3 and 4). The maximum knickpoint drop height is located in the Heping drainage basin; however, compared with the Google Earth image, the location of this knickpoint, which is on the border of cultivated land connecting with lower K_{Sn} values, was identified in the artificial construction. Structures, such as bridges, culverts, and reservoirs, affect longitudinal river profiles derived from DEMs in ways that can either hide features present in reality or

Table 2 The number of drop height ranges, max knickpoint drop heights and the tolerance parameter of extracted knickpoints in each studied drainage basin

Knickpoint drop height (Δz) (m)	Nanao drainage basin	Heping drainage basin	Heren drainage basin	Liwu drainage basin
0–50	60	51	25	–
51–100	18	52	9	54
101–150	3	14	4	23
151–200	2	8	1	15
201–250	–	2	–	5
251–300	–	1	–	7
301–350	–	1	–	2
351–400	–	1	–	2
Max knickpoint drop height (m)	193	365	157	363
Tolerance	22	34	28	64

introduce patterns that do not represent the actual course of the profile (Schwanghart et al. 2013). If we eliminate this knickpoint, which is not generated from nature, the maximum knickpoint drop height is located in the Liwu drainage basin (Table 2).

4.3 K_{sn} values along the river channel

In steady-state river systems that are in equilibrium with tectonic, climatic, or other environmental conditions, the river longitudinal profile can be modeled by a single combination of the steepness index and concavity. Otherwise, in transient systems or river reaches, where the stream profile forms abrupt changes in the channel gradient, convex reaches may be found (Ahmed et al. 2018). Based on Eq. (4), a means of determining the channel slope has been corrected for the expected dependence of the profile gradient on the drainage area. One can determine the K_{sn} value that allows for an effective comparison of the profiles of streams with significantly varying drainage areas (Wobus et al. 2006). In this study, the K_{sn} value was calculated the same reference concavity value ($\theta_{ref} = 0.45$) for all the studied drainage basins. The range of K_{sn} values for the four drainage basins and their corresponding recorded pixel numbers shown in Table 3. The largest K_{sn} values of the Nanao, Heping, Heren and Liwu drainage basins were 626, 1123, 667, and 1442, respectively.

Because the distribution of the K_{sn} value range is wide (0–1450), the recorded pixel numbers of K_{sn} values were not distributed equally in each range (Table 3). We attempt to classify K_{sn} values into five classes in order to reveal the variation of K_{sn} values clearly (Fig. 5). There are many K_{sn} values in class 1 distributed in the Nanao drainage basin, particularly in the lithology of alluvium, Lsc Formation, and Ns Formation. In the central and southern region of the Nanao drainage

Table 3 The number of K_{sn} values for hundredth interval calculated along the river channel in each studied drainage basin

K_{sn} value range	Nanao drainage basin	Heping drainage basin	Heren drainage basin	Liwu drainage basin
0–100	6615	7181	558	5995
101–200	3873	10,020	1016	15,945
201–300	691	2521	500	4990
301–400	152	730	132	1578
401–500	46	243	40	521
501–600	11	92	14	175
601–700	4	29	8	98
701–800	–	14	–	59
801–900	–	12	–	40
901–1000	–	10	–	13
1001–1100	–	5	–	11
1101–1200	–	1	–	9
1200–1300	–	–	–	5
1300–1450	–	–	–	6
Total number	11,392	20,858	2268	29,445

basin, more K_{sn} values appear in classes 1 and 2, and the K_{sn} value in classes 3 and 4 are partially displayed along the lithological boundary (Figs. 5 and 6a). In the Heping and Heren drainage basins, most K_{sn} values fall between class 2 and 4, particularly in the south of the Heping drainage basin and many parts of the Heren drainage basin, reflecting the higher K_{sn} values in class 3 and 4. For the Liwu drainage basin, the number of streams with higher K_{sn} values (class 4 and 5) is greater than that of other drainage basins (Table 3), and most streams at higher elevations on the west side (Fig. 3) exhibit lower K_{sn} values (Fig. 6d).

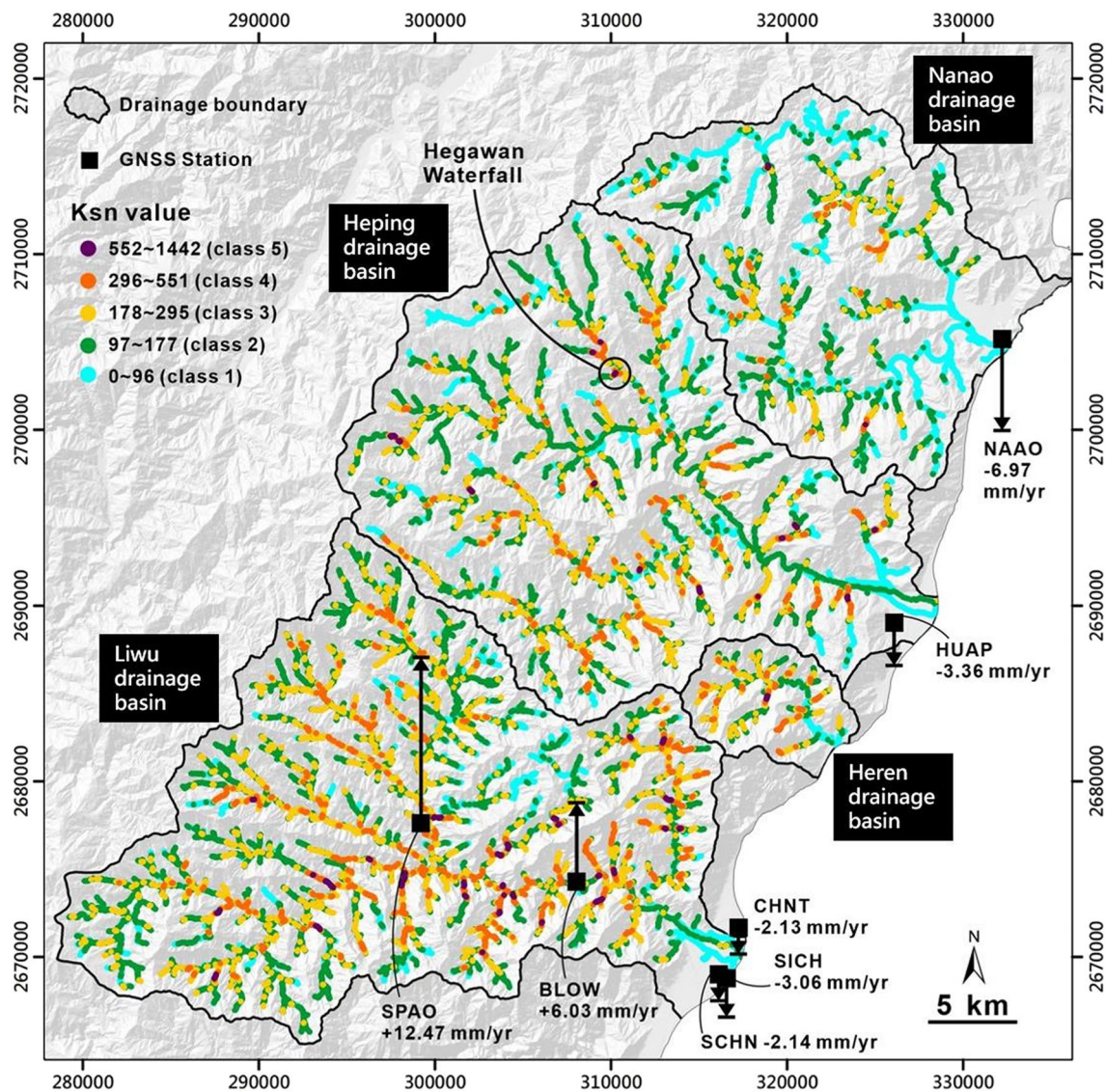


Fig. 5 The K_{sn} value distribution with different classes (from 1 to 5) along the river channel. The black squares represent the location of continuous GNSS stations. The observation period of these GNSS stations have been sustained for more than 15 years. The observation period of each station is as follows: NAAO (2004.04–2021.07), HUAP (2004.05–2021.07), CHNT (2004.01–2021.07), SICH (2005.12–2020.12), SCHN (2004.01–2021.07), BLOW (2006.06–2021.07), and SPAO (2004.04–2021.07)

5 Discussion

Climatic and tectonic perturbations induce a response in the channel profiles as they adjust towards a new equilibrium profile. The transient response of the channel to perturbations caused by multiple factors is characterized by their metrics (i.e., channel steepness and knickpoints) (Marliyani et al. 2016). The topographic steady-state is achieved wherever the long-term erosion rate balances the rock uplift rate, and consequently, the topography is statistically invariant over the long term. In the steady-state, the river channel is not marked by abrupt knickpoints (discrete steps in either the channel elevation or

gradient), and the longitudinal profiles of bedrock rivers are often smoothly concave-up and reasonably well described by the power law relating the local channel gradient to the upstream drainage area (Whipple 2004).

The origin and genesis of knickpoints can be manifold, considering that the present morphology is the result of the interactions of different factors (Marrucci et al. 2018). The generation of knickpoints can be considered to be caused by various factors, such as tectonic movement (including tectonic uplift and offsetting active faults), quaternary glaciations, river captures, variable lithology, base-level changes, and landslide damming (Marrucci

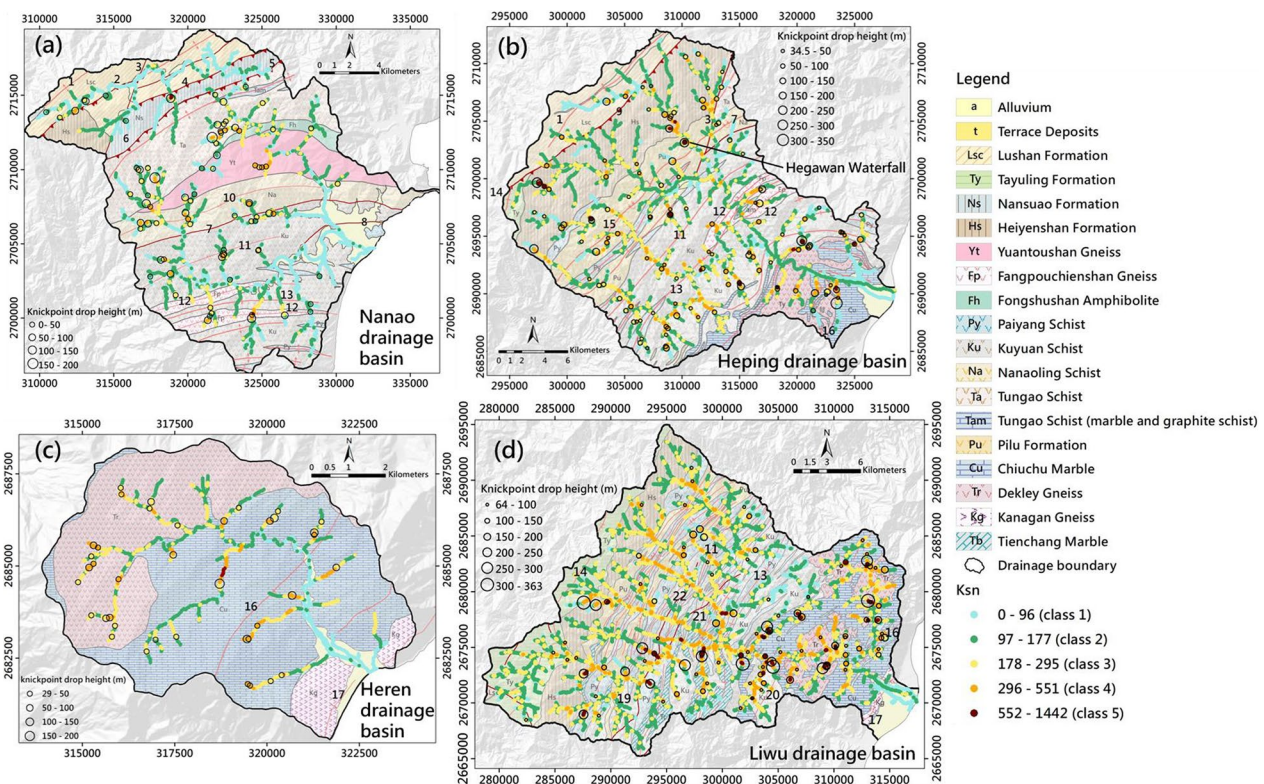


Fig. 6 The locations of extracted knickpoints with K_{sn} value distributions in each drainage basin: **a** the Nanao drainage basin; **b** the Heping drainage basin; **c** the Heren drainage basin; **d** the Liwu drainage basin. The abbreviations indicate the lithological units and the grey lines indicate the individual lithological boundaries

et al. 2018; Ahmed et al. 2019). Although the erosion activity caused by climatic factors can influence the competition between drainage areas and subsequently affect the symmetry of drainage divides, gradually leading the drainage system to adjust to an equilibrium state over time (He et al. 2021). However, the weathering process is an exogenic processes that operates on a short timescale, making it difficult to discuss in such case. Shrestha and Gani (2022) also pointed out that due to the lack of paleoclimate data, it could not link climate factors between the distribution of knickpoints when investigating their spatial variation. In this study, we consider long-term perturbations caused by endogenetic process on river channels, as described in the following sections such as geologic lineament structure, varying lithology, base-level fall and uplift activity, potential rupture.

Analysis of channel gradients and longitudinal profiles provides a promising means of exploring the spatial distribution of rock uplift in an actively deforming orogen (Kirby and Whipple 2001; Snyder et al. 2000). The K_{sn} value, which is used as a topographic indicator, has been shown by many researchers to correlate with rock lift and lithology (Wobus et al. 2006; Kirby and Whipple 2012; Whipple et al. 2013). Because the selection

algorithm of knickpoints in TopoToolBox2 is not normalized for the drainage area, the largest knickpoint selected may not correspond to the largest changes in channel steepness (Gailleton et al. 2019). The drop height of each knickpoint can be obtained by adjusting the iteration calculation of the river longitudinal profile. The magnitude of the knickpoint drop height can reflect the extent of abrupt changes in the river longitudinal profile. The location of the extracted knickpoints was also accompanied with the K_{sn} value changes along the connecting river channel. Therefore, if we consider the locations of knickpoint together with the spatial distribution of the K_{sn} value, we can then synthesize to discuss the perturbations that were caused by possible factors in river longitudinal profile.

5.1 River channel response to geologic lineament structure

The spatial distribution of knickpoints and their proximity to structural features such as folds and faults can be used to determine whether the knickpoints are formed in response to differential uplift or merely because the channel is adjusted to non-tectonically derived changes such as lithologic resistance to erosion

(Marliyani et al. 2016). To observe an overview of knickpoint distributions relevant to the geological structure, the extraction of knickpoints in each drainage basin projected with lineament structure extension, such as faults, anticlines, and synclines from the geological map (Fei and Chen 2013), are shown in Fig. 6. The results show that some knickpoints are partially situated along the lithological contact boundary or geological lineament structure.

In reality, the lithological contact boundaries and geological structures due to the rugged terrain might not extend to continuous and linear alignment as the geological map displays on the surface. This may cause non-linear fitting of the knickpoints close to the lineament structure. The characteristics of large lineaments are marked by numbers, such as the Tsueyfenghu fault (No. 2) and Lupihsi fault (No. 7) in the Nanao drainage basin (Fig. 6a), and the Kulu fault (No. 3) in the northeast of the Heping drainage basin (Fig. 6b). Each of these lineaments has knickpoints with a lower drop height located close to some sections of the fault. In addition, the structures of the Lupihsi Synclinorium (No. 10) in the Nanao drainage basin also exhibits this phenomenon.

However, the lineament of the Tsueyfenghu, Kulu, and Lupihsi faults also stretch superimposing with the lithological boundary, and the generation of knickpoints may be caused by dual factors (lithological boundary and fault) accompanied by the K_{sn} value variation. On the left side of the Kulu fault in the Heping drainage basin, there is a partial stream with higher K_{sn} value, and the larger knickpoint, which is identified as topographic features “Hegawan Waterfall” located nearby, downstream (Figs. 5 and 6b). Based on the distribution of another large knickpoint and clusters of knickpoints in the upstream river channel, as well as significant variation in the K_{sn} value in this segment of river channel, it exhibits similar variations pattern in K_{sn} values on the right side where the Kulu fault (No. 3) passes through. Furthermore, upon comparing with the geological map, other rivers in the northern of the Heping drainage basin that flow through the boundary between Hs and Pu Formations do not show significant variations in K_{sn} values due to varying lithology. Therefore, we assumed that this location could be affected by the rupture, which is still unknown yet. From the distribution pattern of knickpoints, most of them in the Nanao and Heping drainage basins spread disorder, which could be related to the lithological contact boundary or geologic lineament structure.

5.2 River channel response to varying lithology

It has been widely recognized that varying lithologic resistance to erosion can exert a strong influence on the channel gradient and landscape morphology (Hack 1957, 1973; Moglen and Bras 1995; Tucker and Slingerland 1996; Kirby and Whipple 2001). Lithology is considered one of the most important factors affecting the longitudinal profiles of streams, especially in the sedimentary cover where many different lithotypes are present (Marucci et al. 2018). In eastern Taiwan, there is an existing interaction between surface deformation (subsidence and uplift). Although a large part of the area undergoes tectonic forcing, some areas begin to weaken the northward compressive forcing. Our study area has been reported to experience collision waning, mountain collapse, and knickpoint formation, which is controlled by non-tectonic related lithological differences with the lowest K_{sn} value (Chen et al. 2015).

The distribution of knickpoints can assist in identifying the possible lithological contact boundary, and the average K_{sn} value also reflects the different lithologic resistances. This indicates that varying lithology influences the landscape morphology of the river longitudinal profile. In some cases, lithology clearly influences channel steepness, as harder and less fractured rocks are often associated with steeper channels (Duvall et al. 2004). The different rock properties of each lithological unit may have caused a sudden change in erodibility at the boundaries. In addition, the K_{sn} value may be influenced by various erodibility factors when the river flows over different rock units (Chen et al. 2015).

According to previous research (Chen et al. 2015), rivers such as the Nanao and Heping Rivers in northeastern Taiwan are reaching gradation, and the generation of knickpoints is mainly controlled by lithology. To determine the relationship between the lithological unit and the K_{sn} value distribution in individual drainage basin, the segment of the average K_{sn} value was divided by different lithological units in this study (Fig. 7). The lithological unit bordered with grey lines was taken from the geological map (Fei and Chen 2013; see also the legend of Fig. 1b). The average K_{sn} value of some streams flowing through certain lithological units that exposed less area (Table 4, asterisked “*”) is underrepresented. The highest average K_{sn} value of the lithological units of the Nanao, Heping, Heren, and Liwu drainage basins were found in the lithology of Fp Gneiss, Tr Gneiss, and Cu Marble, respectively (Fig. 7). It can be observed that streams crossing a transition in rock strength develop higher K_{sn} values (Duvall et al. 2004). It is particularly noteworthy that gneiss (Fp and Tr) corresponded with a higher average K_{sn} value than other lithology units between these drainage basins (Table 4).

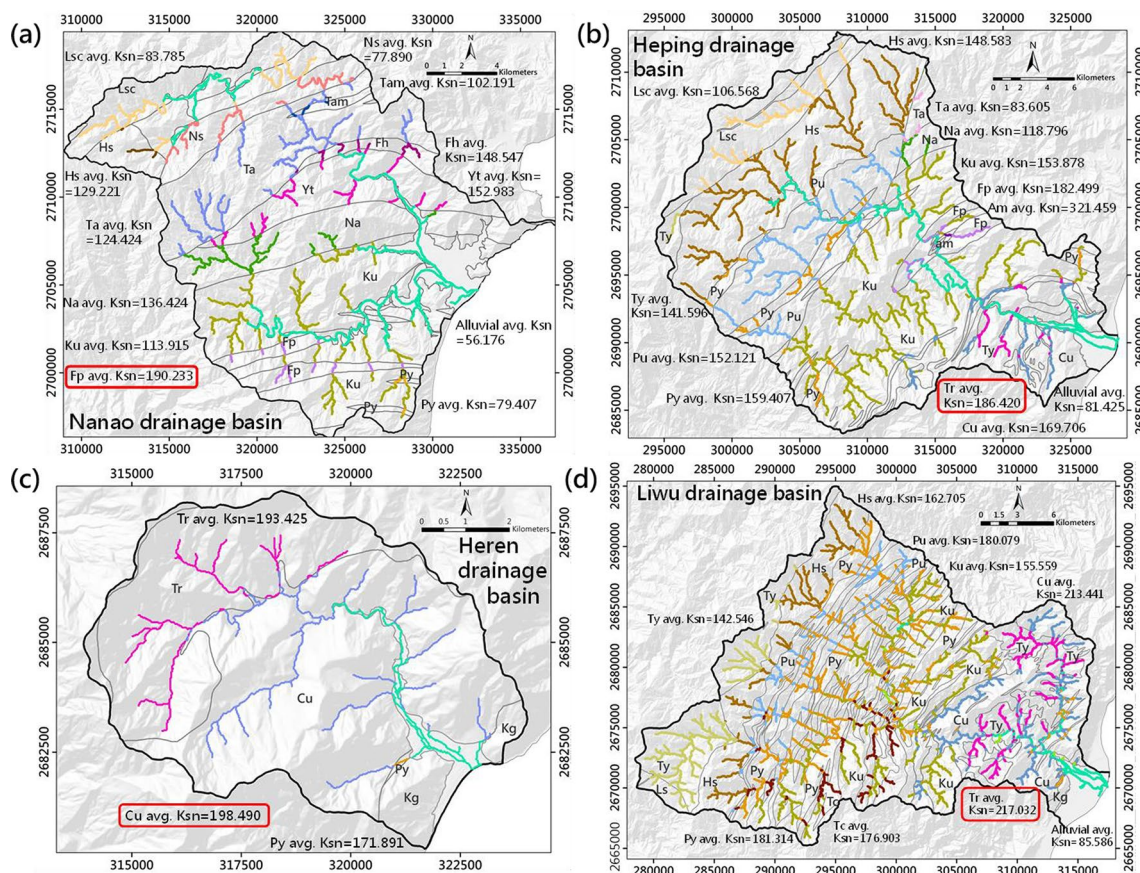


Fig. 7 The streams flow through various lithological units in each drainage basin and the average K_{sn} value calculated from these divided streams segments: **a** the Nanao drainage basin; **b** the Heping drainage basin; **c** the Heren drainage basin; **d** the Liwu drainage basin. The abbreviations indicate the lithological unit and the grey lines indicate the individual lithologic boundaries. The streams on the same lithology types display the same colors in these drainages

On the other hand, the spatial distribution of lower K_{sn} values through most of the Nanao drainage basin might reflect that the rock uplift was not the main activity in this region. The K_{sn} values in classes 3 and 4 continuously spread along the lithologic boundary, such as the Fh Amphibolite, Yt Gneiss, and Fp Gneiss (Fig. 6a). Several knickpoints are gathered in the vicinity, forming a cluster adjacent to the lithologic boundary of the Fh Amphibolite and Yt Gneiss, and the configuration of this cluster distribution seems to surround the lithologic boundary. To the south, another area is significantly affected by lithology. The double narrow band shape of the Fp Gneiss from east to west is the cause of several knickpoints and the K_{sn} value varies parallel arrangement across the boundary of the Fp Gneiss.

On the southeastern side of the Heping drainage basin, the Tr Gneiss and Cu Marble lithological units are the primary distributed rock types. Although there are many artificial mining area constructions in this region, several parallel streams with knickpoints and K_{sn} values varying

between class 3 and class 5 may have been generated from the lithological boundary of the Tr Gneiss and Cu Marble (Fig. 6b). The distribution of the K_{sn} value may also reflect the pattern of Tr Gneiss on the ground surface, which does not exactly match its depicted shape on the geological map. Another region that reveals the existence of Fp Gneiss on the geological map in the Heping drainage basin also contributed towards the K_{sn} values in classes 3 and 4, as well as the knickpoint generation close to the boundary of the Fp Gneiss.

The K_{sn} value distribution in the Liwu drainage basin also had the highest K_{sn} value compared to other study drainage systems. The east side of the Liwu drainage basin consists of a large area of Tr Gneiss and Cu Marble, and the stream channels flow through these two lithologies, reflecting the higher K_{sn} value variation in classes 3 to 5 (Fig. 6d). These two types of lithologies were calculated to have larger average K_{sn} values in the Liwu drainage basin (Table 4). Furthermore, several places on the boundary of gneiss and marble attribute a larger drop

Table 4 The average K_{Sn} value associated with different lithological units in each study drainage basin

Geological time	Lithological unit	Nanao drainage basin	Heping drainage basin	Heren drainage basin	Liwu drainage basin
Average K_{Sn} value					
Holocene	Alluvium(a)	56.176	81.425	54.316	85.586
	Terrace Deposits(t)	–	–	–	112.702
Miocene	Lushan (Lsc) Formation	83.785	106.568	–	–
	Chingshuihu Member	–	–	–	–
Eocene–Oligocene	Tayuling (Ty) Formation	–	141.596*	–	142.546
	Nansuao (Ns) Formation	77.890	–	–	–
Late Paleozoic–Mesozoic	Heiyenshan (Hs) Formation	129.221*	148.583	–	162.705
	Pilu (Pu) Formation	–	152.121	–	180.079
	Yuantoushan (Yt) Gneiss	152.983	–	–	–
	Fangpouchienshan (Fp) Gneiss	190.233	182.499	–	–
	Fongshushan (Fh) Amphibolite	148.547	–	–	–
	Paiyang (Py) Schist	79.407*	159.407	171.891*	181.314
	Kuyuan (Ku) Schist	113.915	153.878	–	155.559
	Chiuchu (Cu) Marble	–	169.706	198.490	213.441
	Nanaoling (Na) Schist	136.424	118.796*	–	–
	Tungao (Ta) Schist	124.424	83.605*	–	–
Marble (and graphite schist) (Tam)	Marble (and graphite schist) (Tam)	102.191*	–	–	–
	Kanagan (Kg) Gneiss	–	–	–	70.314*
	Dekley (Tr) Gneiss	–	186.420	193.425	217.032
	amphibolite (am) body	–	321.459*	–	–
Tienchang (Tc) Marble	–	–	–	176.903	

The numbers with an asterisk "*" indicate that the pathway of stream channels flowing through this kind of lithology are shorter and underrepresented

height of knickpoints, which may arise from the relatively greater strength of lithology resistance.

5.3 River channel response to base-level fall and uplift activity

Tectonic activity plays an important role in the river longitudinal profile response of the studied drainage basins. The Nanao drainage basin enters the collapse post-collision zone, and the WEP boundary projected across through the Heping and Liwu drainage basins may induce uplift and subsidence on the surface in these areas. Therefore, regional activity and intensity can be evaluated from variations in K_{Sn} values, which can provide a sensitive measure of the uplift rate (Wang et al. 2019). From the distribution of knickpoints, the magnitude of knickpoint drop height and the variation in K_{Sn} values in medium to high classes can also observe the influence of long-term uplift tendency in the studied drainage basins (Figs. 3 and 4).

In the Nanao drainage basin and north of the Heping drainage basin, most streams have lower K_{Sn} values (classes 1 to 2) distribution with smaller knickpoints, except some part of the streams with medium to high K_{Sn} values (classes 3 to 5) which are attached to larger

knickpoints caused by the lineament structure or lithologic boundary. Although the structures and variable lithology are the dominant factors that generated the knickpoints in the Nanao drainage basin and north of the Heping drainage basin, there may be other factors related to base-level changes that cannot be neglected. The knickpoints of the Nanao drainage basin have a lower magnitude drop height and are symmetrical along the upstream of the Nanao South Stream (Fig. 3b, red dotted circle); the knickpoints along the Dazhuoshui Stream of the Heping drainage basin also exhibit this phenomenon (Fig. 3c, red dotted circle). This could be because these regions experience base-level lowering that gradually induces knickpoint propagation upstream of higher elevation. The knickpoint clusters, as independent waves of the bedrock incision, actively propagate through the drainage network. This phenomenon resembling knickpoint propagation as a kinematic wave has been reported in the southern Appalachians (Gallen et al. 2013). This indicates that this area is represented through a lower-actively adjustment.

To the south of the Heping basin and Liwu drainage basin, the streams generally exhibit higher K_{Sn} values. Compared with the northern part of the Heping drainage

basin, more knickpoints are densely distributed in the southern part of the Heping drainage basin (Fig. 3a). In the Liwu drainage basin, many higher magnitude knickpoints with medium to high K_{sn} values (classes 3 to 5) were distributed along the main tributaries (stream order 3) spreading in the middle-upper reaches that were induced by uplift activity (Fig. 5). Many upstream reaches of the Liwu drainage basin appeared to have fewer knickpoints (Fig. 3a) because most knickpoints have not propagated to the upstream reaches, which implies that this area is undergoing uplift and the activity continues. In addition, according to a previous geodetic survey, the in situ measurement route passing through the Liwu area reflected the tendency of uplift over decades (Ching et al 2011).

Public data regarding continuous GNSS measurements were obtained from the TGM (Taiwan Geodetic Model) platform (<http://tgm.earth.sinica.edu.tw/index.php>), which was gathered by Institute of Earth Sciences (IES), Academia Sinica. The vertical velocity observation is dependent on the calculation from the records of the GNSS stations (Fig. 5, the locations marked with black squares) in the studied drainage basins. The vertical velocity, which adopted the trend after removing seasonal and earthquake effects on GNSS observations is -6.97 mm/yr (NAAO), -3.36 mm/yr (HUAP), -2.13 mm/yr (CHNT), -3.06 mm/yr (SICH), -2.14 mm/yr (SCHN), 6.03 mm/yr (BLOW), 12.47 mm/yr (SPA0). From north to south in the study area, the vertical velocity tended to progressively experience subsidence to uplift. In the Liwu drainage basin, the vertical velocities of GNSS stations

show both tendencies, especially in mountainous areas that have increased uplift velocity. Another data related to the field investigation of previous study (Hsieh et al. 2013) also showed the cross sections of river terraces along the Liwu River consisting of a series of terraces. The cross-section profiles of the Liwu River we derived from DEM reveals high relief and steep valleys (Fig. 3 profile L-L' and Fig. 4e), which manifest the long-term incision trend of the river in response to rock uplift. The bedrock incision rate of Liwu river reported > 10 mm/yr (and likely > 20 mm/yr) (Hsieh et al. 2013). According to these data, the tendency of tectonic activity could correspond to the clear variation in the K_{sn} value (classes 3 to 5) along most of the main tributaries in Liwu drainage basin.

5.4 River channel response to potential rupture on the surface

The variation in the K_{sn} value may reflect a small rupture on the surface locally. Two micro-seismic swarms exist under the shallow ground in the Heren and Liwu drainage basins (Fig. 8), and the seismicity could cause potential ruptures on the surface. In the Heren drainage, the Cu Marble exhibited a higher average K_{sn} value than the Tr Gneiss (Fig. 7 and Table 4). However, this type of gneiss lithology has a higher average K_{sn} value than marble and schist in other drainage basins. This could be due to the potential rupture on the surface that results in the highest K_{sn} value in the center of the Heren drainage basin (Fig. 6c) and further promotes a higher average K_{sn} value in the Cu Marble. A shallow (< 5 km depth)

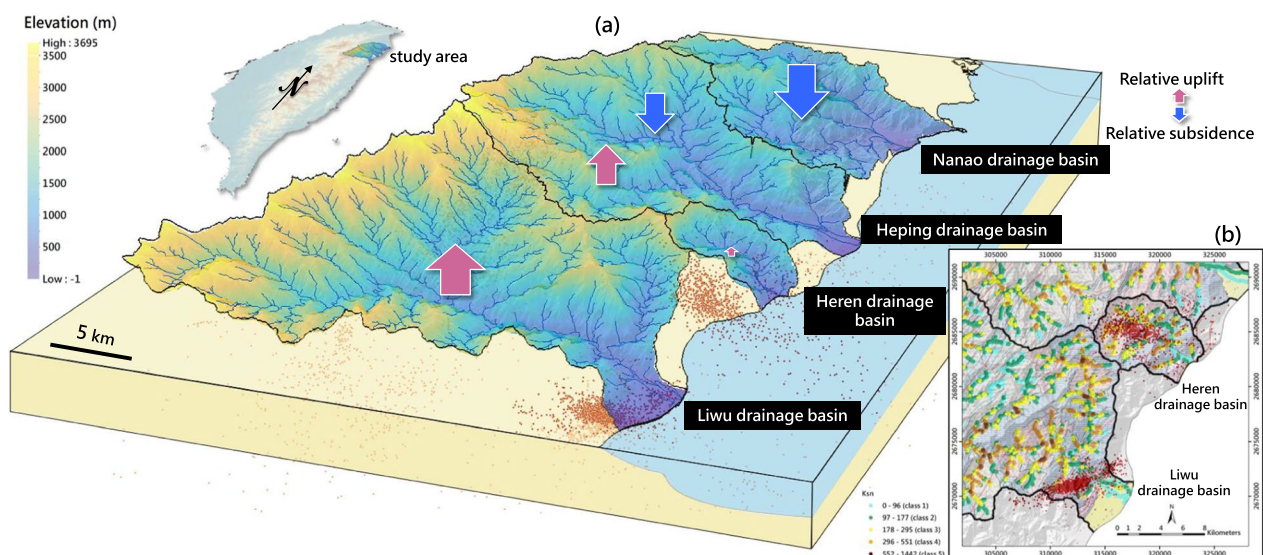


Fig. 8 a the landscape evolution model diagram in the studied drainage basins; b the distribution of micro-seismic swarms projected on the surface in the Heren and Liwu drainage basins. The micro-seismic swarms, which was obtained from Central Weather Bureau (CWB), occurred in 2012–2019

micro-seismic swarm under the Heren drainage basin was discovered (Fig. 8a) and projected in the WNW-ESE direction on the surface (Fig. 8b). The magnitude of the seismicity was mostly smaller than M_w3 . Streams with higher K_{sn} value segments appear in the center of the Heren drainage basin, and the cause could be the displacement on the ground surface induced by potential rupture at shallow depths.

In the Liwu drainage basin, there is also a micro-seismic swarm projected in the ENE-WSW direction on the surface, which approaches the location of the river into the alluvial fan (Fig. 8b). The spatial distribution of this swarm is shallow (<4 km depth) with declining underground in the northwest direction, and the magnitude of seismicity is smaller than M_w3 . The magnitude of most micro-seismicity in the Liwu drainage basin was smaller than that in the Heren drainage basin, but the swarm was denser with an obvious inclination (Fig. 8a). Streams near the northwest side of this swarm show K_{sn} value (classes 3 to 5) variations (Fig. 5), but this local area also shows the pattern of Tr Gneiss exposure. The K_{sn} value variation in this local area may have been induced by this swarm and lithology. We suggest that this may have a small potential for local rupture.

5.5 Landscape evolution model

Base on the river longitudinal profile response in the studied drainage basins, several factors cause perturbations in the river channels. The spatial distribution of the knickpoints and the K_{sn} values along the rivers reveal anomalously steep channels and suggest that the zones were associated with tectonic activity. Additionally, drainage basins are affected by potential ruptures near the surface. In the study area, tectonic forcing act on a large area, but potential ruptures may induce displacement in the local area. The landscape evolution model was generalized based on the result of the geomorphic indices in the studied drainage basins (Fig. 8). Micro-seismic swarms that may induce potential ruptures were discovered in the Heren and Liwu drainage basins at shallow depths. Both swarms were extended in different directions projected on the surface. In the Heren drainage basin, the deformation of slight uplift is considered to be on the southeast side of the swarm, whereas in the Liwu drainage basin, deformation from slight uplift may occur on the northwest side of the swarm (Fig. 8b).

The drainage basins affect by different tectonic forcings from north to south, which can be reflected in the long-term incision of the river into the bedrock. In the north of the study area (the Nanao drainage basin and northern part of the Heping drainage basin) undergoes base-level lowering; in contrast, the south of the study area (southern part of the Heping drainage basin

and the Liwu drainage basin) is still in the process of tectonic uplift (Fig. 8a). The uplift tends to gradually increase from the south of the Heping drainage basin to the Liwu drainage basin. However, the uniform tectonic forcing in the entire studied drainage area could influence tilting differently in each drainage basin, especially in the area affected by uplift activity. Uplift activity may have induced the tilting of the Heping drainage basin from south to north. Because most of the Liwu drainage basin is under the influence of uplift, particularly, on the south side, it appears to tilt from southwest to northeast. Moreover, the most upstream reaches on the west side of the Liwu drainage basin have fewer knickpoints at present, and its stream order is the highest among the studied drainage basins. This implies that tectonic activity still prevails south of the study area. The river network of the Liwu drainage basin will develop continuously, and knickpoints will propagate to the upstream reaches in the future.

6 Conclusion

This study attempted to explore geomorphic indices to discuss the long-term tendency of landscape evolution in the Nanao, Heping, Heren and Liwu drainage basins. The possible factors causing perturbations in the river longitudinal profile were lineament structures, lithology, base-level falling, and tectonic uplift in the studied drainages. Based on long-term geomorphic indices and recent observations, analysis results can be concluded as follows:

- (1) The knickpoint is the location in the river longitudinal profile where there is an abrupt change in the gradient of the river channel. In the studied drainage basins, knickpoints can be generated due to geotectonic variables, including lineament structures or lithological contacts. This phenomenon seems to have emerged from knickpoints with lower drop heights and the K_{sn} value variation along the lithological contact boundary or geologic lineament structure in the Nanao and Heping drainage basins.
- (2) The K_{sn} value may be influenced by various erodibilities owing to the different rock properties, which may cause a sudden change in erodibility at the boundaries. One factor causing the higher channel steepness is the presence of various lithologies. Gneiss and marble are the most resistant rocks, reflecting higher average K_{sn} values in the study area. Above all, Fp Gneiss, Tr Gneiss, and Cu Marble corresponded with higher average K_{sn} values than other lithological units among the studied drainage basins.

- (3) Tectonic activity also plays a profound role in influencing the studied drainage basins. From north to south, the drainage basins have been affected by different tectonic forces. The north of the study area undergoes base-level lowering; in contrast, the south of the study area is still in the process of tectonic uplift. The Heping drainage basin, which reflects both the tendencies of subsidence and uplift, is located in the transition zone affected by tectonic activity.
- (4) Both micro-seismic swarms at shallow depths may induce potential rupture in the Heren and Liwu drainage basins. Corresponding to the variation of K_{SN} value in the local area of both drainage basins, slight displacements may exist on the ground and potential ruptures may be locally affected.

Acknowledgements

The authors thank C. W. Chung for helping figure-drawing.

Author contributions

Conceptualization, CYY; methodology, CYY and TWH; formal analysis, CYY and TWH; writing—original draft preparation, CYY; writing—review and editing, all; visualization, CYY, CPC and TWH; supervision, CPC. All authors have read and agreed to the published version of the manuscript.

Funding

This research received no external funding.

Availability of data and materials

The functions library TopoToolBox2 used to calculate in this study are openly available at <https://topotoolbox.wordpress.com/>. DEM analyzed during the current study were derived from the following public domain resources: <https://data.gov.tw/dataset/35430>.

Declarations

Ethics approval and consent to participate

Not applicable.

Consent for publication

Not applicable.

Competing interests

The authors declare that they have no competing interests.

Received: 5 September 2022 Accepted: 7 July 2023

Published online: 31 July 2023

References

- Ahmed MF, Rogers JD, Ismail HE (2018) Knickpoints along the upper Indus River, Pakistan: an exploratory survey of geomorphic processes. *Swiss J Geosci* 111:191–204
- Ahmed MF, Ali MZ, Rogers JD, Khan MS (2019) A study of knickpoint surveys and their likely association with landslides along the Hunza River longitudinal profile. *Environ Earth Sci* 78:15
- CGS (Central Geological Survey), 2016: Zoning of landslide-landslip geologically sensitive area (In Chinese), L0017 Hualien County, 27 pp
- Chen YW, Shyu JBH, Chang CP (2015) Neotectonic characteristics along the eastern flank of the Central Range in the active Taiwan orogen inferred from fluvial channel morphology. *Tectonic* 34:2249–2270
- Chen WS, Yu HS, Yui TF, Chung SL, Lin CH, Lin CW, Yu NT, Wu YM, Wang KL (2016) An introduction to the geology of Taiwan, Geological Society of Taiwan, p 205.
- Ching KE, Hsieh ML, Johnson KM, Chen KH, Rau RJ, Yang M (2011) Modern vertical deformation rates and mountain building in Taiwan from precise leveling and continuous GPS observations, 2000–2008. *J Geophys Res* 116(1–16):B08406
- Duvall A, Kirby E, Burbank D (2004) Tectonic and lithologic controls on bedrock channel profiles and processes in coastal California. *J Geophys Res* 109:18
- Fei L-Y, Chen M-M, (2013) Geological survey and database establishment of upstream catchment areas in flood-prone areas, Central Geological Survey, MOEA, 192.
- Gaillardon B, Mudd SM, Clubb FJ, Peifer D, Hurst MD (2019) A segmentation approach for the reproducible extraction and quantification of knick-points from river long profiles. *Earth Surf Dyn* 7:211–230
- Gallen SF, Wegmann KW, Bohnenstiehl DB (2013) Miocene rejuvenation of topographic relief in the southern Appalachians. *GSA Today* 23:4–10
- Hack JT (1957) Studies of longitudinal stream profiles in Virginia and Maryland. U.S. Geol Survey Prof Paper 294:45–97
- Hack JT (1973) Stream profile analysis and stream-gradient index. *J Res US Geol Surv* 1:421–429
- He C, Yang CJ, Turowski JM, Rao G, Roda-Boluda DC, Yuan XP (2021) Constraining tectonic uplift and advection from the main drainage divide of a mountain belt. *Nat Commun* 44:10
- Howard AD, Dietrich WE, Seidl MA (1994) Modeling fluvial erosion on regional to continental scales. *J Geophys Res Solid Earth* 99:13971–13986
- Hsieh ML, Chyi SJ, Liu CS, Liew PM, Tsai H (2013) Late Holocene fluvial aggradation and bedrock incision in an active mountain belt, Li-wu River, eastern Taiwan, the Project Report of National Science Council of Taiwan, NSC93–2116-M-002–007, 45.
- Jaiswara NK, Kotluri SK, Pandey P, Pandey AK (2020) MATLAB functions for extracting hypsometry, stream-length gradient index, steepness index, chi gradient of channel and swath profiles from digital elevation model (DEM) and other spatial data for landscape characterisation. *Appl Comput Geosci* 7:100033
- Kirby E, Whipple KX (2001) Quantifying differential rock-uplift rates via stream profile analysis. *Geology* 29:415–418
- Kirby E, Whipple KX (2012) Expression of active tectonics in erosional landscapes. *J Struct Geol* 44:54–75
- Marliyani GI, Arrowsmith JR, Whipple KX (2016) Characterization of slow slip rate faults in humid areas: Cilandiri fault zone, Indonesia. *J Geophys Res Earth Surf* 121:2287–2308
- Marrucci M, Zeilinger G, Ribolini A, Schwanghart W (2018) Origin of knick-points in an alpine context subject to different perturbing factors, stura valley, maritime alps (North-Western Italy). *Geosciences* 8:443
- Moglen GE, Bras RL (1995) The effect of spatial heterogeneities on geomorphic expression in a model of basin evolution. *Water Resour Res* 31:2613–2623
- Palézieux L, Leith K, Loew S (2020) Planform river channel perturbations resulting from active landsliding in the High Himalaya of Bhutan, *Earth Surf Dyn*, under review.
- Perron JT, Royden (2013) An integral approach to bedrock river profile analysis. *Earth Surf Proc Land* 38:570–576
- Schwanghart W, Scherler D (2014) Short communication: topotoolbox 2-MATLAB-based software for topographic analysis and modeling in Earth surface sciences. *Earth Surf Dyn* 2:1–7
- Schwanghart W, Scherler D (2017) Bumps in river profiles: uncertainty assessment and smoothing using quantile regression techniques. *Earth Surf Dyn* 5:821–839
- Schwanghart W, Groom G, Kuhn NJ, Heckrath G (2013) Flow network derivation from a high resolution DEM in a low relief, agrarian landscape. *Earth Surf Process Landf* 38:1576–1586
- Shrestha N, Gani ND (2022) Quantitative tectonic geomorphic study from bedrock rivers of the fold and thrust belt in the Bengal Basin. *Geol J* 58:1325–1725
- Simoes M, Sassolas-Serrayet T, Cattin R, Le Roux-Mallouf R, Ferry M, Drukpa D (2021) Topographic disequilibrium, landscape dynamics and active tectonics: an example from the Bhutan Himalayas. *Earth Surf Dyn* 9:895–921

- Snyder NP, Whipple KX, Tucker GE, Merritts DJ (2000) Landscape response to tectonic forcing: digital elevation model analysis of stream profiles in the Mendocino Triple Junction region, northern California. *Geol Soc Am Bull* 112:1250–1263
- Strahler AN (1952) Hypsometric (area-altitude) analysis of erosional topography. *Geol Soc Am Bull* 63:1117–1142
- Su PL, Chen PF, Wang CY (2019) High resolution 3-D p wave velocity structures under NE Taiwan and their tectonic implications. *J Geophys Res Solid Earth* 124:11601–11614
- Tucker GE, Slingerland R (1996) Predicting sediment flux from fold and thrust belts. *Basin Res* 8:329–349
- Wang J, Hu ZB, Pan BT, Dong ZJ, Li XH, Li XQ, Bridgland D (2019) Spatial distribution pattern of channel steepness index as evidence for differential rock uplift along the eastern Altun Shan on the northern Tibetan Plateau. *Global Planet Change* 181:102979
- Whipple KX (2004) Bedrock rivers and the geomorphology of active orogens. *Annu Rev Earth Planet Sci* 32:151–185
- Whipple KX, Tucker GE (1999) Dynamics of the stream-power river incision model: Implications for height limits of mountain ranges, landscape response timescales, and research needs. *J Geophys Res Solid Earth* 104:17661–17674
- Whipple KX, DiBiase RA, Crosby BT (2013) 9.28 bedrock rivers, treatise on geomorphology. Academic Press, San Diego, pp 550–573
- Wobus C, Whipple KX, Kirby E, Snyder N, Johnson J, Spyropoulou K, Crosby B, Sheehan D (2006) Tectonics from topography: procedures, promise, and pitfalls, Tectonics, Climate, and Landscape Evolution. *Geol Soc Am Spec Pap* 398:56–75
- Wu FT, Liang WT, Lee JC, Benz H, Villasenor A (2009) A model for the termination of the Ryukyu subduction zone against Taiwan: a junction of collision, subduction/separation, and subduction boundaries. *J Geophys Res* 114:B07404
- Yu S-B, Chen H-Y, Kuo L-C (1997) Velocity field of GPS stations in the Taiwan area. *Tectonophysics* 274:41–59
- Zhou L, Liu W, Chen X, Wang H, Hu X, Li X, Schwanghart W (2021) Relationship between dams, knickpoints and the longitudinal profile of the upper Indus river. *Front Earth Sci* 9:18

Publisher's Note

Springer Nature remains neutral with regard to jurisdictional claims in published maps and institutional affiliations.

Submit your manuscript to a SpringerOpen[®] journal and benefit from:

- Convenient online submission
- Rigorous peer review
- Open access: articles freely available online
- High visibility within the field
- Retaining the copyright to your article

Submit your next manuscript at ► [springeropen.com](https://www.springeropen.com)
